CUORE: a cryogenic underground observatory for rare events

C. Arnaboldi[a], F.T. Avignone III[b,*], J. Beeman[c,j], M. Barucci[d], M. Balata[e], C. Brofferio[a], C. Bucci[e], S. Cebrian[f], R.J. Creswick[b], S. Capelli[a], L. Carbone[a], O. Cremonesi[a], A. de Ward[g], E. Fiorini[a], H.A. Farach[b], G. Frossati[g], A. Giuliani[h], D. Giugni[a], P. Gorla[a], E.E. Haller[c,j], I.G. Irastorza[f], R.J. McDonald[c], A. Morales[f], E.B. Norman[c], P. Negri[a], A. Nucciotti[a], M. Pedretti[h], C. Pobes[f], V. Palmieri[i], M. Pavan[a], G. Pessina[a], S. Pirro[a], E. Previtali[a], C. Rosenfeld[b], A.R. Smith[c], M. Sisti[a], G. Ventura[d], M. Vanzini[a], L. Zanotti[a]

[a] Dipartimento di Fisica dell'Università di Milano-Bicocca e Sezione di Milano dell'INFN, I-20136 Milan, Italy
[b] Department of Physics and Astronomy, University of South Carolina, Columbia, SC 29208, USA
[c] Lawrence Berkeley National Laboratory, Berkeley, CA 94720, USA
[d] Dipartimento di Fisica dell'Università di Firenze e Sezione di Firenze dell'INFN, I-50125 Firenze, Italy
[e] Laboratori Nazionali del Gran Sasso, I-67010 Assergi (L'Aquila), Italy
[f] Laboratorio de Fisica Nuclear y Altas Energias, Universidàd de Zaragoza, 50009 Zaragoza, Spain
[g] Kamerling Onnes Laboratory, Leiden University, 2300 RA Leiden, Netherlands
[h] Dipartimento di Scienze Chimiche, Fisiche e Matematiche dell'Università dell'Insubria e Sezione di Milano dell'INFN, I-22100 Como, Italy
[i] Laboratori Nazionali di Legnaro, Via Romea, 4, I-35020 Legnaro (Padova), Italy
[j] Department of Materials Science and Mineral Engineering, University of California, Berkeley, CA 94720, USA

For the CUORE Collaboration

Abstract

CUORE is a proposed tightly packed array of 1000 TeO_2 bolometers, each being a cube 5 cm on a side with a mass of 760 g. The array consists of 25 vertical towers, arranged in a square of 5 towers×5 towers, each containing 10 layers of four crystals. The design of the detector is optimized for ultralow-background searches: for neutrinoless double-beta decay of ^{130}Te (33.8% abundance), cold dark matter, solar axions, and rare nuclear decays. A preliminary experiment involving 20 crystals $3 \times 3 \times 6$ cm^3 of 340 g has been completed, and a single CUORE tower is being constructed as a smaller-scale experiment called CUORICINO. The expected performance and sensitivity, based on Monte Carlo simulations and extrapolations of present results, are reported.
© 2003 Elsevier B.V. All rights reserved.

---

*Corresponding author.

1. Introduction

Neutrinoless double-beta decay, is a process in which two neutrons in a nucleus might beta decay by exchanging a virtual Majorana neutrino, each emitting an electron. This process violates lepton number conservation ($\Delta L = 2$) [1], and requires neutrinos to be Majorana particles. There are many reviews on the subject [2–5]. The decay rate for the process involving the exchange of a Majorana neutrino can be expressed as follows:

$$\frac{1}{\tau_{1/2}^{0\nu}} = G^{0\nu}(E_0, Z)$$
$$\times \frac{|\langle m_\nu \rangle|^2}{m_e^2} |M_f^{0\nu} - (g_A/g_V)^2 M_{GT}^{0\nu}|^2. \qquad (1)$$

In Eq. (1), $G^{0\nu}$ is the two-body phase-space factor including coupling constants, $M_f^{0\nu}$ and $M_{GT}^{0\nu}$ are the Fermi and Gamow–Teller nuclear matrix elements, respectively; g_A and g_V are the axial-vector and vector relative weak coupling constants, respectively, and m_e is the electron mass. The quantity $|\langle m_\nu \rangle|$ is the effective Majorana electron neutrino mass given by

$$|\langle m_\nu \rangle| \equiv | |U_{e1}^L|^2 m_1 + |U_{e2}^L|^2 m_2 e^{i\phi_2}$$
$$+ |U_{e3}^L|^2 m_3 e^{i\phi_3}| \qquad (2)$$

where $e^{i\phi_2}$ and $e^{i\phi_3}$ are Majorana CP phases (± 1 for CP conservation) and $m_{1,2,3}$ are the mass eigenvalues.

The electron neutrino, for example, is a linear combination of neutrino mass eigenstates, i.e.

$$|\nu_e\rangle = U_{e1}^L |\nu_1\rangle + U_{e2}^L |\nu_2\rangle + U_{e3}^L |\nu_3\rangle. \qquad (3)$$

The effective Majorana neutrino mass, $|\langle m_\nu \rangle|$, is directly derivable from the measured half-life of the decay as follows:

$$|\langle m_\nu \rangle| = m_e \frac{1}{\sqrt{F_N \tau_{1/2}^{0\nu}}} \quad (eV) \qquad (4)$$

where $F_N \equiv G^{0\nu} |M_f^{0\nu} - (g_A/g_V)^2 M_{GT}^{0\nu}|^2$. This quantity derives from nuclear structure calculations and is model dependent as shown later.

The most sensitive double-beta decay experiments thus far utilize germanium detectors isotopically enriched in ^{76}Ge from 7.8% abundance to $\sim 86\%$. This activity began with natural abundance Ge detectors by Fiorini et al. [6] in Milan evolving over the years to the first experiments with small isotopically enriched Ge detectors [7], and finally to the two present multi-kilogram isotopically enriched ^{76}Ge experiments: Heidelberg–Moscow [8] and IGEX [9,10].

Where should the field of double-beta decay go from here? Suppose we consider the observed neutrino oscillations in the data from atmospheric neutrinos [11] and solar neutrinos [12]. These, coupled with the recent exciting results reported by the Sudbury Neutrino Observatory (SNO) Collaboration [13], gives clear evidence that solar neutrinos oscillate, and that the standard solar model is correct, but that solar electron neutrinos are oscillating to other flavors on their way from the sun, or in the sun. In addition, neutrino oscillation experiments have yielded the following values of $|U_{ek}|^2 : |U_{e1}|^2 = (0.75^{+0.07}_{-0.12})$, $|U_{e2}|^2 = (0.25^{+0.12}_{-0.07})$, and $|U_{e3}|^2 = (< 0.026)$ with confidence levels of 3σ.

A number of recent theoretical interpretations of these data [14–19] imply that the effective Majorana mass of the electron neutrino, $|\langle m_\nu \rangle|$, expressed in Eq. (2), could be in the range 0.01 eV to the present bounds [8,10]. Considering this range, could a next generation $0\nu\beta\beta$-decay experiment detect it? If so, what technique would be the best for a possible discovery experiment? We will address these questions in an effort to demonstrate that CUORE, an array of 1000, 760 g TeO_2 bolometers, is one of the best approaches presently available. It can be launched without isotopic enrichment nor extensive Research and Development (R & D), and it can achieve next generation sensitivity.

The CUORE project, discussed in Section 2 is a natural extension of the successful MI-DBD ^{130}Te experiment [20] where for the first time a large array of bolometers was used to search for $0\nu\beta\beta$-decay. The good results obtained so far prove that the *bolometric* technique, although novel, is a competitive alternative to the traditional *calorimetric* Ge technique. In Section 2, details of the detectors of the CUORE array are discussed, while in Section 3, the cryogenic system required to cool the array at the operating temperature of ~ 10 mK is described. Background issues are considered in

Section 4, while electronics, DAQ and data-analysis are discussed in Sections 5 and 6. The background simulation and the predicted sensitivity for CUORE are analyzed in Section 7 where we also discuss briefly the physical potential of CUORE regarding dark matter and solar axions searches. In Section 8, the enrichment option is discussed.

2. The CUORE project

The CUORE detector will consist of an array of 1000 TeO_2 bolometers arranged in a square configuration of 25 towers of 40 crystals each (Fig. 1). The principle of operation of these bolometers is now well understood [21]. Tellurium oxide is a dielectric and diamagnetic material. According to the Debye Law, the heat capacity of a single crystal at low temperature is proportional to the ratio $(T/T_\Theta)^3$, where T_Θ is the Debye temperature of TeO_2. Thus, providing that the temperature is extremely low, a small energy release in the crystal results in a measurable temperature rise. This temperature change can be recorded with thermal sensors and in particular using Neutron Transmutation-Doped (NTD) germanium thermistors. These devices were developed and produced at the Lawrence Berkeley National Laboratory (LBNL) and UC Berkeley

Department of Material Science [22]. They have been made uniquely uniform in their response and sensitivity by neutron exposure control with neutron absorbing foils accompanying the germanium in the reactor [23].

The TeO_2 crystals are produced by the Shanghai Quinhua Material Company (SQM) in Shanghai, China and they will be the source of 760 g TeO_2 crystals for CUORE [24]. A single CUORE detector consists of a $5 \times 5 \times 5$ cm^3 single crystal of TeO_2 that acts both as a detector and source. The detectors will be supported in a copper frame in the 25 tower configuration shown in Fig. 1. The frame, and dilution refrigerator (DR) mixing chamber to which it is thermally connected, forms the heat sink, while the polytetrafluoroethylene (PTFE) or TEFLON stand-offs provide the thermal impedance which delays the re-cooling of the bolometers. The bolometers operate at ~ 10 mK.

A single tower of CUORE is presently under construction. It will be attached to the mixing chamber of the same DR used in the Milano 20 crystal array experiment (MI-DBD) and run not only as a test bed for CUORE but will also be an experiment called CUORICINO [24,25] (which in Italian means small CUORE) designed to improve on the .present sensitivity of $|\langle m_v \rangle|$ obtained with isotopically enriched Ge detectors [8,9]. CUOR-ICINO will prove the feasibility of the extension of
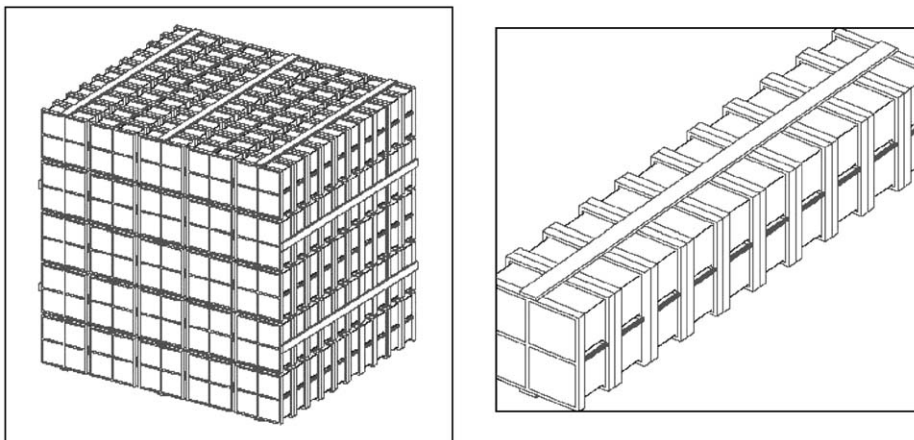

Fig. 1. The CUORE detector (left), one of the 25 towers (right).

the MI-DBD technology to large arrays. The smaller array of 20 $3 \times 3 \times 6$ cm^3 crystals was operated successfully for 31,000 h kg. The data yield a bound $T_{1/2}^{0\nu}(^{130}\text{Te}) > 2 \times 10^{23}$ years, corresponding to $|\langle m_\nu \rangle| < (1 \ or \ 2)$ eV, depending on the nuclear matrix element used [20].

The CUORE detector then will be the final version of a three-step development comprising MI-DBD, CUORICINO, and finally CUORE. This, plus the fact that CUORE requires no isotopic enrichment (the isotopic abundance of the $\beta\beta$ emitter ^{130}Te is 33.8%), puts CUORE ahead of other options of truly next generation $0\nu\beta\beta$ experiments. The technology, though novel, is developed and to a large degree proven.

2.1. The single CUORE detector

A single CUORE detector is a $5 \times 5 \times 5$ cm^3 single crystal of TeO$_2$ grown with ultrapure TeO$_2$ powders and optically polished on the surfaces. Crystals of TeO$_2$ have a tetragonal structure, and are grown along the (0 0 1) axis. The two axes normal to this axis are crystallographically equivalent, a fact relevant to their use in the search for solar axions discussed later [26]. The surface hardness is not the same for all sides, which complicates the crystal polishing. We have shown that repeated thermal cycling does not damage the crystals, as in the cases of crystals of other tellurium compounds, or those of tellurium metal. The Debye temperature of the TeO$_2$ crystals was specially measured for the CUORE project as 232 K [27]. This differs from the previous value of 272 K in the literature [28]. The specific heat of the TeO$_2$ crystals was found to follow the Debye law down to 60 mK; the heat capacity of the 760 g crystals is 2.3×10^{-9} J/K extrapolated down to 10 mK.

The NTD thermistors are attached by epoxy to the crystal and are operated in the Variable Range Hopping (VRH) conduction regime with a Coulomb gap [29–31]. The most important parameter characterizing the thermal response is the sensitivity, A, defined as follows:

$$A = \left| \frac{\text{d} \log R}{\text{d} \log T} \right| = \gamma \left(\frac{T_0}{T} \right)^\gamma. \tag{5}$$

For our NTD thermistors, this parameter ranges between 7 and 10. The resistance behavior follows the relation

$$R = R_0 \exp(T_0/T)^\gamma, \quad \gamma = \tfrac{1}{2}. \tag{6}$$

The VRH regime occurs in Ge when it is "doped" close to the Metal-to-Insulator Transition, which is $\sim 6 \times 10^{16}$ atoms/cm^3. This is achieved by thermal neutron radiation in a nuclear reactor, resulting in (n, γ) reactions on ^{70,72,73,74,76}Ge, followed by β^--decay or electron capture. To first order, this produces (for a natural Ge sample) the following stable isotopes: ^{71}Ga(18%), ^{73}Ge(8.3%), ^{74}Ge(36%), ^{75}As(12%), and ^{77}Se(0.8%). Beta minus and electron capture lead to n and p dopants, respectively. The sensitivity parameter, A, depends on the neutron irradiation dose. Therefore, each thermistor must be characterized at operating temperatures, as described for Si thermistors by Alessandrello et al. [32].

It is very important to optimize the neutron irradiation exposure and to make the exposures as uniform as possible. It is not possible to evaluate the thermistor material directly from the reactor because of the long half-life of ^{71}Ge (11.43 days). A delay of several months is required to see if the Ge needs more exposure. To circumvent this difficulty, the Ge material is accompanied by foils of metal with long-lived (n, γ) radioactive daughter nuclides. Accordingly, the neutron exposure of the Ge can be determined accurately, and uniformity of exposure is achieved. This technique was developed recently by the LBNL group of the CUORE Collaboration [23]. Following the neutron exposure and radioactive decay period, the NTD germanium is first heat treated to repair the crystal structure then cut into $3 \times 3 \times 1$ mm^3 strips. The thermistors are glued to the TeO$_2$ crystal by nine spots of Araldit rapid, Ciba Geigy epoxy, of 0.4–0.7 mm deposited on the crystal surface by an array of pins. The height of each spot is 50 μm. This procedure was found to be reliable and reproducible in the MI-DBD experiment [20]. The heat conductance of the epoxy spots was measured in Milan and the phenomenological relation was found to be $\sim 2.6 \times 10^{-4}(T(\text{K}))^3$ W/K/spot.

The stabilization of the response of bolometers is crucial because of the unavoidable small variations in the temperature of the heat bath that change the detector gain (and consequently deteriorates the energy resolution). This problem is successfully addressed by means of a Joule heater glued on to each crystal. The heater is used to inject a uniform energy in the crystal and the thermal gain is monitored and corrected off-line (see Section 6). The heaters are Si chips with a heavily doped meander structure with a constant resistance between 50 and 100 kΩ. They are manufactured by the ITC-IRST company in Trento, Italy.

Electrical connections are made with two 50-μm-diameter gold wires, ball bonded to metalized surfaces on the thermistor. The gold wires are crimped into a copper tube, which is inserted into a larger one forming the electrical connection, and avoiding low-temperature solder which contains ^{210}Pb and traces of other radioisotopes. The larger copper tube, ~ 14 mm long and 2 mm in diameter, is glued to the copper frame that supports the crystals. This tube is thermally connected to the frame but electrically insulated.

The mounting of the TeO$_2$ crystals is crucial to detector performance, and must fulfill a number of sometimes contradictory criteria:

(1) the crystals must be rigidly secured to the frame to prevent power dissipation by friction caused by unavoidable vibrations, that can prevent the crystal from reaching the required temperature and can produce low-frequency noise;
(2) the thermal conductance to the heat sink (copper frame) must be low enough to delay the re-cooling of the crystal, following a heat pulse, such that the pulse decay time (re-cooling time) is much longer than the rise time;
(3) however, the heat conductance must be high enough to guarantee efficient cooling;
(4) the frame must compensate for the differences in thermal expansion co-efficients of the various materials used;
(5) and finally, only materials selected for low radioactivity can be used.

For CUORE, only two materials will be used, copper and PTFE; they can both be obtained with very low levels of radioactivity. Copper has a thermal conductivity and specific heat high enough to be an ideal heat bath, and has excellent mechanical properties; it machines well, and has excellent tensile, tortinal and compressional strength.

PTFE is used between the copper frame and the crystals. It has low heat conductance and low heat leak [33]. It compensates for the differences between coefficients of thermal expansion of copper and of TeO$_2$. The heat conductance between the crystal and heat sink was measured in a similar configuration, but with a contact area larger by a factor of 2 [34].

The measurements of the temperature dependence of specific heats and thermal conductivities is crucially important for developing a model that explains detector performance and that can be used to improve the detector design.

2.2. The detector model

A rough approximation of the NTD thermistor voltage pulse amplitude ΔV_{bol} produced by an energy deposition E into the TeO$_2$ absorber can be obtained by

$$\Delta V_{bol} = V_{bol} A \frac{\Delta T_{bol}}{T_{bol}} = V_{bol} A \frac{E}{C T_{bol}} \tag{7}$$

where V_{bol} is the bias of the NTD thermistor, A is the sensitivity obtained from Eq. (5), ΔT_{bol} is the temperature increase and C is the heat capacity of the absorber. Using the heat capacity discussed earlier, a 1 MeV energy deposition into the TeO$_2$ absorber results in $\Delta T_{bol} = 7 \times 10^{-5}$ K. Using Eq. (7), this results in $\Delta V_{bol} \sim 600$ μV; however, the observed pulses are lower by a factor ~ 5, therefore a more quantitative model is needed.

A semi-quantitative Thermal Model (TM) has been developed which describes the detector in terms of three thermal nodes with finite heat capacities, the TeO$_2$ crystal absorber, Ge thermistor lattice, and Ge thermistor electrons. For simplification, the lattice component of heat capacity is assumed to be negligible. The network describing the detector is shown in Fig. 2. The two
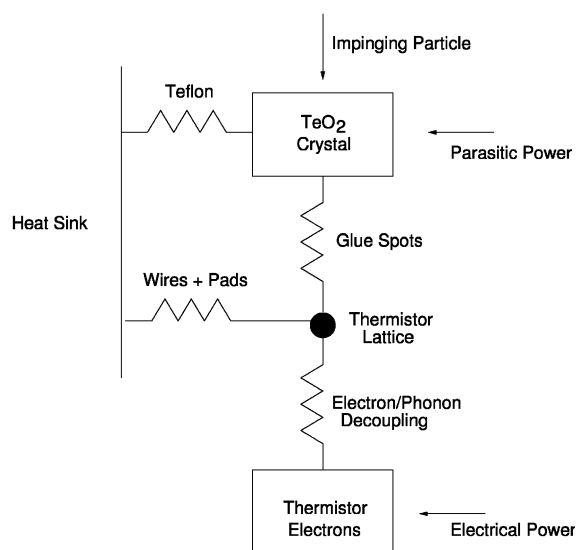
Fig. 2. Network representing the detector model.

heat capacities, and four thermal conductances and the parasitic power from the vibrations and power dissipated in the thermistor electrons, are the model parameters. A typical energy deposition of 1 MeV in the crystal is used and it is assumed that it is instantaneously thermalized.

A computer code was developed in Milan to determine the static behavior. The required input data are the heat sink temperature, the temperature behavior of the thermal conductances shown in Fig. 2, the parasitic power in the crystal, and a set of values of electrical joule power dissipated in the thermistor electrons. The code determines a complete solution to the static problem, for each power level, and yields the temperature of the three thermal nodes, the resistance of the thermistor, and the current through it. These parameters define the "operational point". A set of operational points, with a fixed heat sink temperature, defines a "load curve". Load curves are expressed as a set of voltage–current, or power resistance points. When the static operation point is determined, the time evolution of the pulse is computed. The main aim of the TM is to have a reliable prediction of the detector figure of merit on the basis of the known thermal parameters. To address this question, it is necessary to solve the non-trivial problem of how to compare the

performances of two detectors. A more sensitive thermistor would yield larger amplitude pulses, but they are also more sensitive to spurious noise, for example microphonics, cross-talk, and slow heat pulses from vibrations that excite the 1–5 Hz portion of the noise spectrum. More gain at the heat sink temperature yields larger pulses at the price of higher resistance and more spurious noise.

Recent experience shows that the best way to define a detector figure of merit is by fixing the heat sink temperature between 7 and 11 mK and by measuring a load curve. Using particle or heater pulses, the operation point on the load curve, corresponding to the highest signal is determined. For each heat sink temperature, one determines a pair of points, the thermistor resistance, R, and the signal amplitude, V, usually expressed in microvolts per MeV, corresponding to the maximum pulse amplitude for a given heat sink temperature. One obtains a characteristic curve for that detector by plotting voltage vs. resistance, which to a good approximation is a straight line on a log–log plot. This is called the Detector Merit Curve (DMC). Experience shows that a detector has constant signal-to-noise ratio along a DMC. No large differences in performance are noted for heat sink temperatures of 8 or 12 mK, because the signal level and the spurious noised offset one another. It is better to avoid the extremities of the DMC that lead to higher spurious noise or low signals.

The best way to compare two different detectors is by using their DMCs. If the DMC of detector A lies systematically above that of detector B, the performance of detector A is superior. It provides the highest signals for a fixed thermistor resistance value. The main value of the TM is to predict the DMC given the temperature behavior of the thermal parameters discussed above.

As a test of the model, a typical detector of the MI-DBD 20-element array was simulated. These have different masses and geometries than the CUORE crystals. A DMC was then constructed using the model for this detector. It was then compared to the real DMC measured for the 20-detector array. A significant spread among the experimental points, for all 20 detectors was
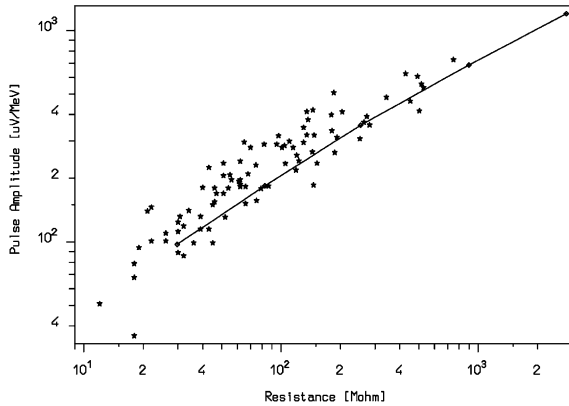
Fig. 3. DMC: simulation and experimental points for the 20 detector array.

Fig. 4. Real pulses (full line) and simulated pulses (line + points).

found. There were two reasons for this, intrinsic detector differences and the presence of points not corresponding exactly to the maximum signal. Nevertheless, the simulated DMC lies inside of the experimental points and has the correct slope (see Fig. 3). The detector simulations are not distinguishable from a typical detector array.

The TM must correctly predict not only pulse amplitude, but also time constants. At a typical operating resistance (~ 100 MΩ), the predicted rise time (10–90%) and decay time are, respectively, 40 and 430 ms, and lie inside the distribution of these parameters for the 20-detector array. In Fig. 4, the simulated pulse is compared with real pulses collected with four detectors, randomly chosen among the 20 elements. It is evident that the pulse-shape of the simulated detector is very similar to that of a typical array of detectors. From this, it was concluded that the TM is capable of explaining semi-quantitative performance of the 20-element array.

The TM can be used in parallel with specific low-temperature experimental tests, to define the optimum properties of the CUORE element, and the results thus obtained imply the following optimum parameters for the CUORE elements:

(1) TeO$_2$ absorber dimensions: $50 \times 50 \times 50$ mm^3, with a mass of 760 g;
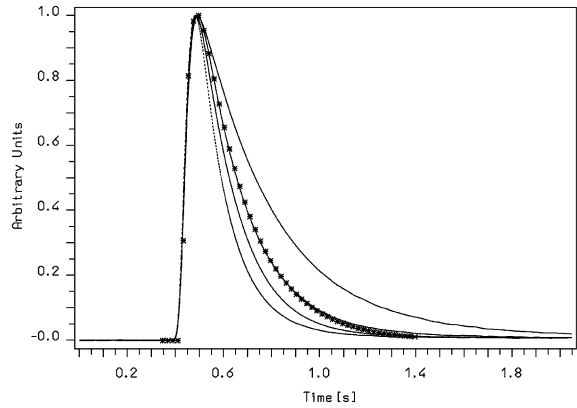(2) NTD Thermistor #31, $T_0 = 3.0$ K, $R_0 = 1.5$ Ω, dimensions $3 \times 3 \times 1$ mm^3, with a contact distance of 3 mm, and with a resistance of 50 MΩ at $T = 10$ mK;
(3) absorber–thermistor coupling made with nine epoxy spots, 0.5–0.8 mm in diameter, and 50 μm high;
(4) gold connecting wires 50 μm in diameter, and 15 mm in length;
(5) crystals mounted on PTFE blocks with a total PTFE-to-crystal contact area equal to about a few square mm.

2.3. The modular structure of the CUORE detector

The CUORE array comprises 1000 TeO$_2$ bolometers, grouped in 250 modules of four bolometers each. These are arranged in 25 towers of 40 crystals each, or a stack 10 modules high. The towers are assembled in a 5×5 matrix as shown in Fig. 1.

The structure of each four-detector module is shown in Fig. 5. The four crystals are held between two copper frames joined by copper columns. PTFE pieces are inserted between the copper and TeO$_2$, as a heat impedance and to clamp the crystals. There is a 6 mm gap between crystals with no material between them.

The four detectors are mechanically coupled; some of the PTFE blocks and springs act simultaneously on two crystals. Tests on this and a similar structure but with $3 \times 3 \times 6$ mm^3 crystals
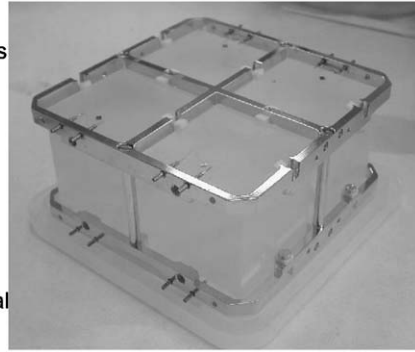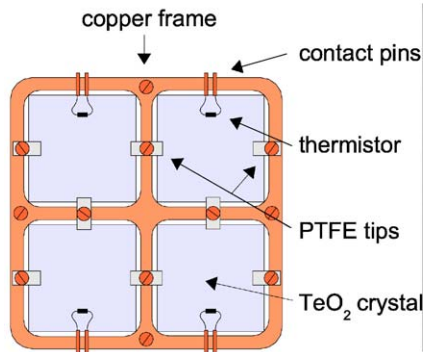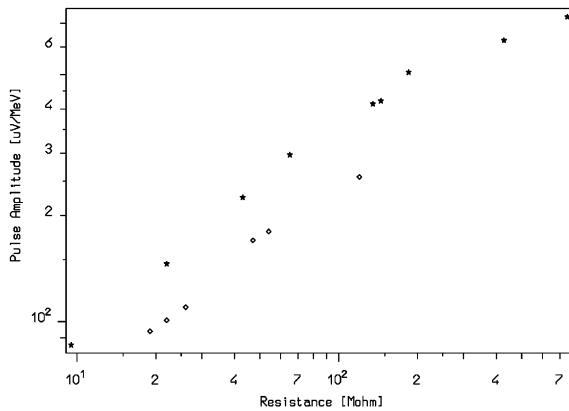
Fig. 5. A four-detector module.

Fig. 6. Improvement in the DMC by increasing the thermistor size: $3 \times 3 \times 1$ mm^3 thermistors (stars) vs. $3 \times 1.5 \times 0.4$ mm^3 (diamonds).
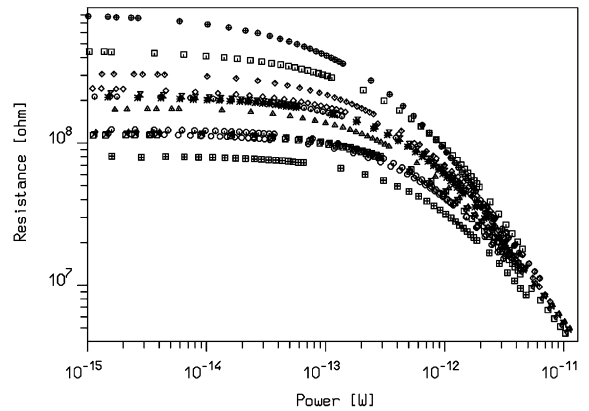
Fig. 8. Fifteen thermistor load curves for the 20 crystal array.
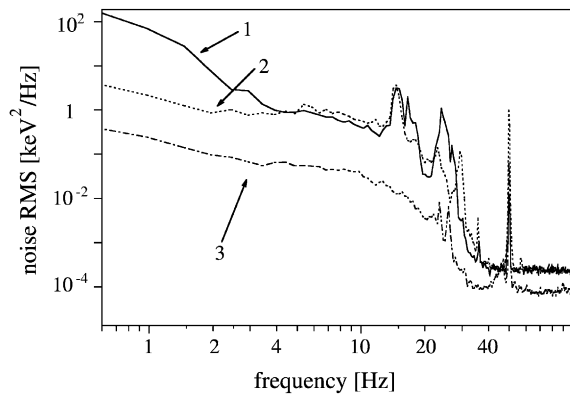
Fig. 7. Noise power spectra without damping suspension (1), with damping suspension only (2) and with damping suspension + cold electronics (3).

clearly demonstrate that the CUORE technology is viable. Noise reduction was achieved by replacing the $3 \times 1.5 \times 0.4$ mm^3 Ge thermistor by one with dimensions $3 \times 3 \times 1$ mm^3, which significantly improved the DMC shown in Fig. 6, and by utilizing cold electronics (Fig. 7).

Reproducibility was tested on the MI-DBD array, which is a significant number of detectors (20) operating simultaneously. The reproducibility is satisfactory as shown in the load curves in Fig. 8. Four-detector modules of $50 \times 50 \times 50$ mm^3 crystals were also successfully tested with pulse amplitudes spanning an interval from 50 to 150 μV/MeV at ~ 100 MΩ operation point, in agreement with the TM. The full-width at half-maximum FWHM is ~ 1 keV for low-energy

gamma peaks, and ~5–10 keV at 2.6 MeV. A stack of 10, four-detector modules, will be connected by two vertical copper bars. The details of the wiring of the towers is still under development; however, the current plan is for 50 μm diameter twisted pairs of nylon-coated constantane wire running along the vertical copper bars. On the top of each tower there would be 40 twisted pairs for the thermistors and four for the heaters. Two more twisted pairs will be required for diagnostic thermometers, one on top and one on the bottom of the tower.

The CUORICINO detector presently under construction consists of one of the 40 detector towers. CUORE is an array of 25 towers, each of which will be suspended independently from a large square copper plate, thermally connected to the mixing chamber of the DR. In this manner, tests of CUORICINO will be tests of the CUORE array. The array will be suspended from the mixing chamber by a vertical spring to decouple the detector from the vibrations of the DR. Tests were performed with piezo-electric accelerometers and vibrators to optimize the suspension (see Fig. 7). As a result, a pendulum mechanical suspension was designed for the entire CUORE array.

The heavy shielding of CUORE will present non-trivial problems in the energy calibration with radioactive sources. The presently considered option is to use radioactive metal wires encapsulated in PTFE tubes. The tubes would be placed vertically between the towers, and free to slide along a fixed tube to the appropriate calibration point. A vacuum tight sliding seal will allow the part of the tube containing wire to be inserted and extracted from the cryostat.

3. The cryogenic system

The CUORE bolometers will operate at temperatures between 7 and 10 mK. This will require an extremely powerful DR. At these temperatures, the cooling power of a DR varies approximately as T^2. Estimates were made of the parasitic power the detector and DR would receive from: heat transfer of the residual helium gas in the inner vacuum chamber (IVC), power radiated from the 50 mK shield facing the detector, and from vibrational energy (microphonic noise).

The estimated value is ~1 μW at 7 mK, using reasonable values for the residual gas pressure and achievable surface quality for radiation transfer. The resulting estimate for the radiation contribution was negligible. CUORE will utilize a similar system to that of the Nautilus Collaboration that cools a 2-ton gravitational antenna. That system experienced a parasitic power of 10 μW from unknown sources.

The CUORE detector will be cooled by an He^3/He^4 refrigerator with a cooling power of 3 mW at 120 mK. Refrigerators with the required characteristics are technically feasible. One example is the DRS-700 DR model constructed by the Kamerling Onnes Laboratory in Leiden. The unit is shown in Fig. 9, inserted in the dewar. One important design feature is the 50-mm-diameter clear access to the mixing chamber to allow a rod, suspended from an external structure, to suspend
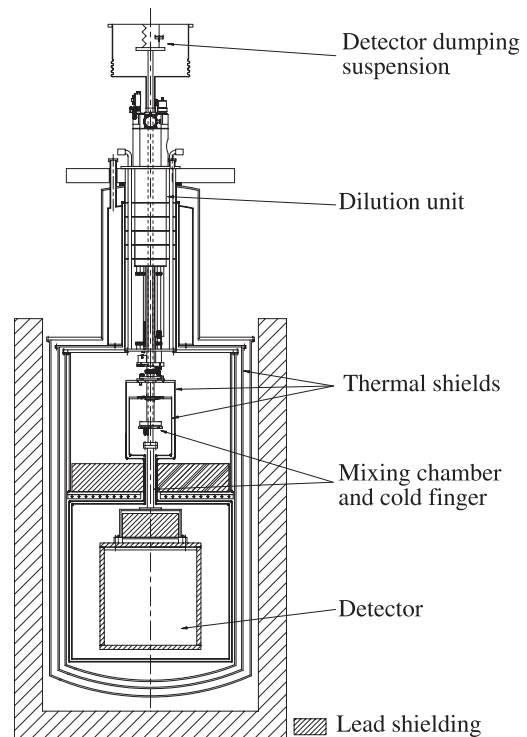

Fig. 9. CUORE cryostat and shielding.

the detector array to minimize vibrations from direct connection to the mixing chamber. The temperature of the rod will be controlled in stages along its length by flexible thermal contacts to avoid vibrations.

The dewar housing the DR will have a jacket of liquid nitrogen (LN) to avoid the need of super-insulation which is not free of radioactivity. The system is designed with several tubes passing through the LN bath, the liquid He bath, and the IVC, to allow refilling with cryogenic liquids, and for sufficient feed through for electrical connections. Liquifiers will provide constant liquid levels for the two baths over long periods of operation.

The He that evaporates from the main bath and from the 1 K-pot will be recovered in a buffer tank and re-liquified with a helium liquifier with a capacity of several tens of l/day. The gas will be cooled to ~ 70 K, then to 10 K, by a two-stage Gifford–MacMahon cycle. This will be followed by a Joule–Thompson cycle that liquifies it and injects it back into the main bath. The nitrogen liquifier, on the other hand, will require only a single-stage Gifford–MacMahon cycle to cool a cold finger above the LN bath. It will condense the evaporated N_2 and let it fall back into the bath.

This complex cryogenic system will require a constant monitoring system. It must be capable of surveying the operating conditions to allow prompt intervention to correct malfunctions rapidly. In addition, the operating conditions of the entire cryogenic system must be recorded for future correlation with instabilities in the experimental data.

4. Radioactivity and shielding

Double-beta decay experiments, as well as dark matter searches and searches for rare events in general, require deep underground locations and ultralow radioactive environments. This latter requirement is usually accomplished by a severe selection of the materials used and by the realization of proper shielding surrounding the detectors. In the case where complicated structures like a DR are used, the problem of shielding and of using only low radioactive contamination materials is complex.

4.1. Shielding

In the case of CUORE, part of the bulk lead shielding will be placed inside of the cryostat, and part outside (Fig. 9). This will shield the dewar, and will reduce the total amount of lead required. A 4π layer of ultralow background lead will constitute 30-cm-thick walls of the cubic structure of the array. This layer will be Roman lead whose ^{210}Pb activity was measured to be less than 4 mBq/kg [35]. The DR will be constructed from materials specially selected for low levels of radioactivity. Nevertheless, these levels might be higher than can be tolerated by the sensitivity requirements.

The top of the detector array will be protected by two layers 1 m × 1 m, with a 10-cm-diameter central bore to accommodate the copper cold finger that supports the detector and the narrow neck of two radiation shields of the refrigerator that are at temperatures of 50 and 600 mK. The layer close to the detector will be 10 cm thick, made from high-quality lead with an activity of 16 Bq/kg of ^{210}Pb. The upper layer, also 10 cm thick, will be made of modern lead with an activity of ^{210}Pb of 150 Bq/kg. Another layer of lead 17 cm thick, and 40 cm × 40 cm will be placed directly on the top face of the detector. It will be constructed from low-activity lead of 16 Bq/kg of ^{210}Pb. This configuration is designed so that the minimum path to the detector from the IVC and the dilution unit is 20 cm of lead. Finally, outside the dewar, there will be two 10 cm thicknesses of lead, 16 Bq/kg of ^{210}Pb for the inner layer, and 150 Bq/kg for the outer layer. The lead shield will be surrounded by a 10-cm-thick box of borated polyethylene that will also function as a hermetically sealed enclosure to exclude radon. It will be flushed constantly with dry nitrogen.

The entire dewar, detector, and shield will be enclosed in a Faraday cage to exclude electromagnetic disturbances that also constitute a source of background, albeit at low energies, important to

dark matter and solar axion searches. The addition of a muon veto surrounding the entire structure will be also considered.

4.2. Material selection and treatment

All the materials used to built the detectors, their mounting structure, the cryostat and the shielding themselves will be selected to ensure that only low radioactive contamination materials will be employed. A particular care will be obviously devoted to the detectors. The TeO_2 crystals will be grown from ultrapure TeO_2 powders to guarantee an extremely low level of bulk contamination (present limit on U and Th contamination is of the order of $\sim 10^{-13}$ g/g). Particular care will be devoted to their surface treatment. Indeed, the first crystals grown by SQM were polished in China with conventional cerium oxide polishing rouge. This resulted in a ^{238}U and ^{232}Th surface contamination of the crystals that contributed to the measured background in the 0νββ of the MI-DBD first run. A re-polishing of the crystals in Italy with low-contamination powders reduced that contamination in the MI-DBD second run. A new polishing process studied in collaboration with SQM and a semi-automatic polishing system developed at LBNL was used for the surface treatment of the CUORICINO crystals (partially done in China and completed in Italy). Also copper and PTFE used to construct the CUORE array will be selected for their low contamination. Once machined, all the copper and PTFE pieces will undergo a surface cleaning procedure that will guarantee the required low level of surface radioactive contamination for those parts that directly face the detectors. The array will be assembled in a low Rn clean room to avoid contamination from Rn daughters.

4.3. Location

CUORE will be located in the underground halls of Laboratori Nazionali del Gran Sasso (L'Aquila, Italy) at a depth of 3400 m.w.e. where the muon flux is reduced to $\sim 3 \times 10^{-8}$ μ/cm^2/s and the neutron flux to $\sim 10^{-6}$ n/cm^2/s.

5. Electronics and data acquisition

The front-end electronics furnishes a bias current to the NTD thermistors and receives and processes the resulting signal-bearing voltage. We are investigating two configurations that differ by the addition of a cold buffer stage inserted between the detector and the room temperature preamplifier in one case. The connection from the thermistors to the electronics is via a shielded twisted pair from 1 to 5 m in length, depending on the final solution adopted. The design of the electronics addresses four major issues. First, it should minimize the noise generated by the biasing circuitry and the preamplifier in the frequency band from ~ 1 Hz to a few tens of Hz. Second, it should accommodate the broad spread of manufacturing characteristics typical of the bolometer and thermistor modules. For some modules, for example, the optimum bias current is as low as 150 pA and for others as high as 300 pA. As a consequence, the signal amplitude exhibits a corresponding spread. Third, it should enable in situ measurement of the bolometer characteristics. Fourth, the design should incorporate a high level of remote programmability to allow adjustments required during the observing period that do not require mechanical interventions in the vicinity of the bolometers. In the following subsections, we give a brief discussion of the circuitry devised to address these issues. An extended discussion of the electronics appears in Ref. [36].

5.1. Thermistor biasing

Thermistor biasing is achieved by the application of a programmable voltage across a series combination of the thermistor and two load resistors. If the electronic system is operated at room temperature, the load resistors are also at room temperature (R_L in Fig. 10). The contribution to $1/f$ noise of large resistors under bias and the minimization of this noise source is the subject of an independent report [37]. Under computer control, the biasing resistors can be reduced from 27 to 5.5 GΩ which facilitates a measurement of the bolometer's I–V characteristics at large bias. The impedance at the input of the electronics is
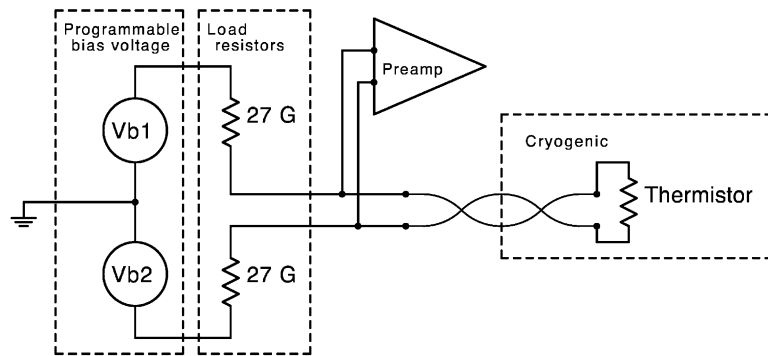
Fig. 10. Functional block diagram of the front-end electronics. Normally, R_L is 27 GΩ. For determination of a bolometer I–V characteristic, a command from the computer can reduce R_L to 5.5 GΩ.

sufficiently high that parasitic conductance in the circuit board demands great attention. Precautions taken to suppress parasitic conductance were (a) segregation of inverting and non-inverting inputs by circuit board layer, (b) strategic placement of guard traces around the solder junctions of high-impedance component leads, (c) maintenance of a minimum spacing of ~ 5 mm between high-impedance traces, and (d) the placement of slots at critical locations on the circuit board to avoid conductance through minute amounts of soldering residue that can escape the standard cleaning procedures. Together these measures yield excellent results.

If a cold buffer stage is adopted, the pair of load resistors R_L of Fig. 10 will be moved close to the location of the buffer itself, which is also at low temperature. Their value will be 27 GΩ. In this case, the rest of the biasing set-up will remain unchanged.

The application of bias voltage to the load resistors is the task of the programmable bias attenuator. This circuit is a 5-bit R-2R ladder network with optical isolation of the digital input. Its outputs are the voltages V_{b1} and V_{b2} appearing in Fig. 10. They take the value:

$$V_{b1} = -V_{b2} = (n/64)(V_+ - V_-),$$

where V_+ and V_- are derived from an Agilent Technologies 6627A system power supply common to all modules. The voltage difference $|V_+ - V_-|$ may be set as high as 60 V and n can be set to

any integer value between 1 and 64. Interposed between the programmable bias attenuator and the load resistors (but not shown in Fig. 10) is a bistable DPDT relay, which allows inverting the polarity of the bias voltage. By reversing the bias voltage during in situ DC characterization, we can account for the thermoelectric effect operating in the leads that connect the front-end electronics to the thermistors. Heavy filtering distributed through the biasing network reduces whatever noise originates from the power system or from the network itself to a negligible level.

5.2. Preamplifier

The design of the preamplifier was influenced by four considerations. First, for the source impedance, and signal characteristics that the bolometer presents, a voltage amplifier is the conventional approach [38]. Its performance is not superior to a charge or current configuration [39], but it allows its inputs to float. Floating inputs make biasing compatible with DC coupling. Second, the leads connecting the preamplifiers with the bolometers operating near 10 mK can be between 1 and 5 m in length. The drawback of these long leads is that they act as antennas for microphonic noise. We address this issue by making the preamplifier input differential. Compared with a single-sided input, the amplifier noise power is double, but for the more troublesome microphonic noise originating in the leads, which

is a common mode, we achieve efficient suppression. The differential configuration also serves to suppress interchannel cross-talk. Third, the signal bandwidth of the bolometers extends from 1 to about 10 Hz, and we require that the amplifier noises, both series and parallel, be minimized in this frequency interval. Fourth, monitoring the baseline of each bolometer and correlating baseline shift with shifts in overall system gain require low thermal drift in the preamplifier.

In addition to the above features, the use of a cold buffer stage can further increase the rejection of microphonic noise by minimizing the high impedance section of the detector's connecting leads.

To address these considerations, the room temperature version of the front end adopted is the circuit shown in Fig. 11a. At the core of the design is the JFET pair J1 and J2, which accepts the differential input. The transistor type for these JFETs was selected to minimize noise, especially at low frequency. The capacitance of the gate of the selected transistor is about 80 pF, which optimizes the tradeoff between low series noise, low parallel noise, and matching to the detector. To minimize parallel noise we establish for each of the JFETs $VDS = I_2 R_g - (I_1 - I_2) R_s/2$ at 0.8 V, the lowest value consistent with adequate gain. The connection of the outputs of the operational amplifiers (op-amp) A3 and A4 through the resistors R_f to the sources of the JFETs closes the feedback loop

and establishes the gain at $(R_f + R_s)/R_s$. With $R_f = 20$ kΩ and $R_s = 91$ Ω the gain is 220 V/V. Neither the input JFETs nor any of the op-amp circuits are individually compensated for thermal drift. This issue is dealt with by trimming the circuit as a whole. One component of the current source in the thermal drift compensation circuit of Fig. 11a is a diode that serves as a thermometer. The magnitude of the coefficient η is proportional to the value of a single resistor, and placement of a shunt determines the sign of η. The preamplifier is operated in a temperature-controlled chamber and η is trimmed to neutralize the uncompensated thermal drift. In this way, we were able to reduce an uncompensated drift as large as 60 to about 0.1 μV/°C.

To further minimize the microphonic noise coming from the length of the leads, we have devised, and are testing, a solution that uses an additional stage of amplification, operated cold, and inserted near the 4.2 K plate of the DR (and therefore much closer to the detectors). Each cold stage is a differential buffer composed by two Silicon JFETs that work in the source follower configuration. Accordingly, the length of the leads that connect the detector to this additional buffer stage is reduced to about 1 m, while the remaining portions of the wires in the direction of room temperature are driven by the low output impedance of the buffer. The buffer stage works at the optimum temperature for Silicon, around
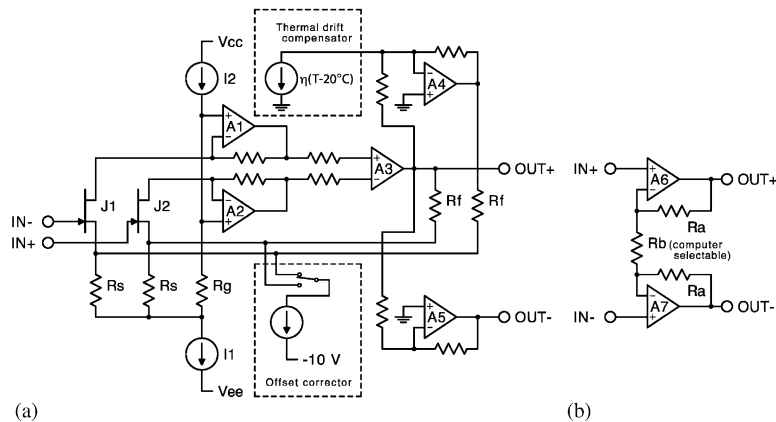

Fig. 11. Schematics of (a) the preamplifier and (b) the programmable gain amplifier.

110 K. Each cold buffer, together with the load resistors, is located on boards that accommodate six channels. The boards are fabricated on a substrate made of PTFE 25% reinforced fiberglass. This solution achieves two goals. First, the small thermal conductance of the PTFE minimizes the injected thermal power needed to increase the temperature of the JFETs to the optimum 110 K, starting from the heat sink at 4.2 K. Second, the radioactivity level of PTFE is lower by a factor of about 2 than that of pure fiberglass. In addition, the printed circuit boards have a thickness of only 0.5 mm to reduce the amount of mass present. Thermally shielded metallic boxes have been constructed, each of which is able to contain two such boards. Inside the boxes, the boards are suspended by means of nylon wires that have a small thermal conductance to the heat sink at 4.2 K. This solution allows a good reduction of noise (see Fig. 7); however, it presents some technical difficulties.

The input offset of the preamplifier, for both configurations, is the sum of contributions from the asymmetry of the JFETs and the bias voltage of the NTD thermistor. The JFET asymmetry may contribute up to ± 20 mV to the offset. In normal operation, thermistor biasing contributes no more than 20 mV, but to obtain the thermistor $I–V$ characteristic, the bias voltage should be adjustable to both polarities to a magnitude as high as 50 mV. The offset corrector circuit is designed to compensate input offsets from -80 to $+80$ mV under the control of the digital section. In a naive design for this circuit, the central element would be a conventional CMOS digital-to-analog converter (DAC). Such a design, however, would generate excessive low-frequency noise. Our design incorporates a DAC8043A, which is less noisy than ordinary DACs because it omits the conventional output buffer. To derive adequate current from this device, we place a low-noise op-amp in the feedback loop. Further noise suppression is achieved with the DAC8043A to swing the output through just 20 mV, i.e. $\frac{1}{4}$ of the maximum output excursion. A simple arrangement of two analog switches in series with low-frequency noise-free resistors provides the necessary additional 60 mV of output swing.

5.3. Programmable gain amplifier

The outputs of the preamplifier drive the differential inputs of the programmable gain amplifier, which is shown in Fig. 11b. The computer can set R_b to any one of 31 parallel combinations of a set of five resistors. The resulting gain from the preamplifier input to the amplifier output takes values from 220 to 5000 V/V. The differential outputs travel on an analog bus to a filter circuit, followed by analog to digital conversion.

The supply voltage for the front end so far described has been designed to have very good stability, of a few ppm/C, and a large rejection ratio [40]. These features provide excellent stability during long-time measurements. One such supply voltage is dedicated to 12 boards, or 24 complete channels.

5.4. Antialiasing filter and analog trigger

In the CUORE experiment, it is feasible to apply optimal filtering algorithms to the detector signal in the off-line analysis, and signal shaping in hardware is thus inappropriate. To ensure adequate frequency response an antialiasing filter is implemented in hardware at the downstream end of the analog signal processing. This low-pass filter is an active six-pole Bessel design, which yields a roll-off of 120 dB/decade. To allow for adapting the bandwidth to the individual bolometer modules the cutoff frequency is adjustable from the computer to 8, 12, 16 or 20 Hz.

The trigger circuit input is AC coupled to the output of the antialiasing filter. Its gain is adjustable from the computer to 4.2, 12.5, 21 or 29 V/V. The AC coupling produces a negative excursion of the trigger circuit input that, if uncompensated, would result in a shift of the baseline. A baseline restoring section [41] in the trigger circuit suppresses this effect. Pulses from a bolometer exhibit a trailing undershoot because of the coupling of the inductive part of the bolometer's dynamic impedance to the parasitic capacitance in shunt with it. After differentiation by the AC coupling, the undershoot of large pulses has the potential to retrigger. An RC network [42]

within the trigger circuit cancels the effect of the undershoot and thus suppresses retriggering. Its time constant is adjustable from the computer to 14, 27, 53, or 66 s. The final element in the trigger circuit is a two-pole Bessel low-pass filter. The cutoff of this filter tracks the cutoff of the antialiasing filter but is higher in frequency by 4 Hz. One trigger-Bessel module accommodates three channels.

5.5. Data acquisition and triggering

The analog trigger and antialising circuits are situated in a small Faraday cage close to the acquisition and triggering system to which they send their outputs. The data acquisition system (DAS) is based on the VXI standard. Its main goal is the implementation of a zero dead-time system based on the continuous analysis of a large circular memory buffer with a very fast data transfer rate (DMA) with the ADC memories. The DAS consists of an embedded controller PC (DASC), and a few trigger and ADC cards. Signals from the front-end electronics are sent to both a series of 16 bit ADC modules (where they are digitized) and, after proper differentiation, to simple threshold trigger modules. The ADC sampling interval is set to values in the range 1–10 ms depending on the observed characteristics of the signals. Because of these large sampling times, each ADC module is multiplexed and can serve a number of acquisition channels. Sampled data are continuously transferred to a large circular buffer of the DASC. When a trigger signal is transferred to the DASC, the circular buffer is analyzed to recognize and extract the desired sampled interval without interfering with the ADC activities. Under normal conditions, this does not require any DAQ deadtime. Synchronization between trigger, the ADC modules and the DASC is of crucial importance. The trigger discriminating thresholds are adjustable in increments of 5 mV. This threshold adjustment, in combination with the gain selection in the trigger circuit provides channel-by-channel fine control of the trigger level. Given the variability of the energy-to-voltage conversion among bolometers, the ability to tailor the trigger level for each bolometer module independently is a valuable feature particularly for dark matter searches for which the trigger level should be as low as possible.

5.6. Noise considerations

When the cold buffer stage is not present, the analog electronics just described produces noise at the level of 50 nV (FWHM) referred to the input over the 10 Hz bandwidth of the signal. The 27 GΩ load resistors produce 80 nV in this bandwidth. The combined noise is then about 100 nV (FWHM). When the cold buffer stage is present the series power noise is increased by a factor of about 2, while parallel noise is decreased by a factor of at least 3, mainly by the use of the cold load resistors. In this way, the overall noise contribution becomes about 90 nV (FWHM). In both cases, the noise is considerably below the 1.0 μV (FWHM) level of noise that we have observed from a reference bolometer that we consider to be an exemplar of good performance. Based on this assessment, we believe that the analog front end is more than adequate for the needs of the experiment.

The two front-end solutions have the same level of noise, but the presence of the cold buffer stage reduces the high impedance path and should further improve the common mode noise from the vibration of the leads. Unfortunately, there is another source of microphonics that is not a common mode. It is caused by the mechanical friction between the detector and its mounting. If this source contributes noise much greater than that of the connecting leads, the use of a cold buffer stage will be not necessary. This would save a factor of two in the number of connecting leads (two for the readout and two for biasing in the case of the cold stage), and will save thermal power injection inside the DR. The savings in parasitic capacitance that is obtained by shortening the high impedance path is not a concern with the very slow signals anticipated.

5.7. Digital control

A digital control system (DCS) enables the computer to manipulate all of the significant

parameters of the analog front end. These parameters include the thermistor bias current, the input offset correction, the gain, and the application of test signals to the inputs. During data acquisition the DCS is generally idle. In this state, even the DCS clock shuts down, thus eliminating the possibility that DCS activity will contribute to noise on the analog outputs.

6. Off-line analysis

When the output voltage of one detector exceeds the trigger threshold, the acquisition system saves a number of converted points of the corresponding channel. Accordingly, for each electronic pulse the wave form corresponding to a time window of approximately 2 s is sampled and acquired. The existence of a pretrigger interval guarantees that a small fraction of the number of points acquired are measurements of the DC level of the detector, or its temperature, just prior to the production of the pulse.

The fact that for each trigger an entire wave form is sampled and recorded implies that off-line analysis of a large body of data will require a significant effort. Nevertheless, this effort will be justified because of the useful information that can be extracted from the signal waveform. The following are important goals for the analysis:

(1) The maximization of the signal-to-noise ratio for the best estimate of the pulse amplitude. This is accomplished by means of the optimum filter (OF) technique [43].
(2) The ability to correct the effects of system instabilities that change the response function of the detectors.
(3) The ability to reject spurious triggered pulses by means of pulse shape analysis.
(4) The capability of identifying and rejecting radioactive background pulses by means of coincidence analysis.

The OF technique is frequently used with bolometers to evaluate the amplitude of a signal superimposed on stochastic noise. This algorithm has proven to provide the best estimate of the pulse amplitude under general conditions. Relative to a simple maximun–minimum algorithm, this technique allows the evaluation of the signal amplitude with much higher efficiency resulting in an improvement in energy resolution by as much as a factor of two. To use the OF technique, the following information is necessary: the response function, i.e. the shape of the signal in a zero-noise condition, and the noise power spectrum. Once these are known, the OF function is determined. It is then used as a software filter for the acquired pulses. The role of the OF function is to weight the frequency components of the signal to suppress those frequencies that are highly influenced by noise. The amplitude of the pulse is then evaluated using optimally filtered pulses. Some pulse shape parameters can be deduced from the comparison of the filtered pulses with the filtered response function.

In processing the data off-line, the following parameters are evaluated and recorded to disk for each digitized pulse:

(1) The *channel number*, i.e. the ADC channel that exceeded the trigger threshold.
(2) The *absolute time* at which the pulse occurs with a precision of 0.1 ms.
(3) The *OF amplitude*, i.e. that of the optimally filtered signals.
(4) The *baseline*, obtained by averaging a proper number of points from the pretrigger interval. This is a direct measurement of the DC level at the output of the detector just prior to the production of the pulse, and therefore provides a measurement of the detector temperature at the creation of the signal.
(5) The signal *rise* and signal *decay times*.
(6) The *pulse shape parameters*, obtained by comparison between the pulse and the expected response function of the bolometer. The algorithms used to make this comparison, and to produce a numerical evaluation of it, are based on two main techniques: the comparison of the wave forms of the pulse and response function after OF, or Adaptive Filtering. A third powerful technique is based on artificial neural networks.
(7) The *pile-up fraction*: Pile up is usually efficiently rejected using pulse shape analysis;

however, this does not guarantee the identification of the rejected event as one from a pile up. To improve this rejection, and to be able to evaluate the fraction of piled-up events, the Wiener–Filter algorithm is implemented [34].

The next step in the off-line analysis is to gain instability correction. The OF amplitudes are corrected to reduce or cancel the effects of system instabilities responsible for the variation of the ratio between the energy, E, absorbed by the crystal and the amplitude, ΔV, of the corresponding electrical pulse. In a very naive model (see Eq. (7)) of bolometers the following relation exists:

$$
\begin{aligned}
\Delta V &= G_{e} A V_{bol} \frac{E}{C T_{bol}} \\
&= G_{e} A V_{bias} \frac{R_{bol}}{R_{bol} + R_{load}} \frac{1}{C T_{bol}} E.
\end{aligned}
\tag{8}
$$

In Eq. (8), G_{e} is the total gain of the electronic chain, A = thermistor sensitivity, V_{bias} = total bias, $V_{bol} = V_{bias} R_{bol}/(R_{bol} + R_{load})$, R_{load} = load resistance, R_{bol} = bolometer resistance, C_{bol} = crystal heat capacity, and T_{bol} = temperature of the crystal.

There are three instabilities that can modify the ratio $\Delta V/E$: a variation in the electronic gain (G_{e}), a variation in the bias (V_{bias}), and finally a variation in the temperature (T_{bol}) of the crystal. The electronic system is designed to guarantee a stability of G_{e} and of V_{bias} within 0.1%. It is, however, much more difficult to maintain stability within 0.1% of the detector temperature over long periods time. At a temperature of 10 mK, this would require maintaining the temperature of 1000 crystals to an accuracy of 10 μK for a period of several days.

To compensate for these instabilities, a silicon resistor glued to each crystal is used as a heater to produce a reference pulse in the detector. It is connected to a high precision programmable pulser that produces a fast voltage pulse every few minutes dissipating the same amount of energy (E_{ref}) into the crystal each time. These voltage pulses mimic pulses produced in the crystal by particle interactions and are used to measure the value of the ratio $\Delta V/E$. Any variation of the amplitude of the reference pulse is due to

variations of $\Delta V/E$. The OF amplitude of the reference pulse is therefore used to measure the actual value of $\Delta V/E$ every few minutes, while the baseline of the reference pulse provides the contemporary measurement of the value of T. A fit is then used to obtain the values of $\Delta V/E$ for each temperature. Therefore, in this step of the off line analysis, the OF amplitude of each pulse is corrected according to the value of $\Delta V/E$ for the detector temperature at which the pulse has been generated. This technique has been proven to be efficient in the MI-DBD experiment, where a typical temperature fluctuation over a day ranged from a few tenths to ∼100 μK. After correction, these fluctuations were reduced to less than 1 μK [44].

Pulse shape analysis is very useful in rejecting spurious signals produced by microphonics and electronic noise. A confidence level is determined for each pulse shape parameter and for the rise and decay time of each pulse. Signals falling within these intervals are defined as "true" pulses, and signals having one or more of their parameters outside of the relevant interval are rejected as noise. The use of more than one pulse shape parameter results in better reliability of the rejection technique.

The linearization of the detector response is critically important for energy calibration. The final step in data processing is the conversion of the OF amplitudes into energy values. The naive bolometer model previously used assumes linearity; however, several parameters depend on the crystal temperature, rendering the corresponding equation non-linear. Accordingly, the relation between ΔV and E will be obtained periodically by the use of radioactive calibration sources. The ratio $\Delta V/E$ will be measured for several gamma-ray lines, and the data will be fit to the model previously described, but taking into consideration the fact that the bolometer resistance and the crystal heat capacity are temperature dependent. This will provide the calibration function of E as a function of ΔV, that will then be used to convert the OF amplitudes into energy values.

Finally, the close-packed array of the crystals will allow the rejection of events that leave energy in more than one crystal. This will be particularly

useful in rejecting a very high-energy gamma rays that enter from outside the array. The small-angle Compton scattering in a single crystal can mimic a double-beta decay event or, a dark matter scattering. The probability that this photon would escape the rest of the array without a second interaction is small. In addition, background events from radioactivity within the structure of the array will also have a significant probability of depositing energy in more than one crystal. This will also be true for high- and intermediate-energy neutrons. In the final stage of off-line analysis, these coincidence events can be identified from the data which will contain the detector number, signal time, pulse energy, and pile-up parameter.

7. Simulation and predicted performances

The goal of CUORE is to achieve a background rate in the range 0.001–0.01 counts/(keV kg year) at the 0νββ transition energy of ^{130}Te (2528 keV). A low counting rate near threshold (that will be of the order of ~ 5 keV) is also predicted and will allow CUORE to produce results in the dark matter arena. In Section 7.1, we present a very conservative evaluation of the background attainable with CUORE; this is mainly based on the status of the art of detector design and of radioactive contaminations. This rather pessimistic approach in background evaluation is the only one that presently guarantees a reliable prediction. However, CUORE construction will require about 5 years; there will therefore be time enough for further R&D dedicated to background reduction as projected in most next generation experiments. This is discussed in Section 7.2.

7.1. Background simulations

Radioactive contamination of individual construction materials, as well as the laboratory environment, were measured and the impact on detector performance determined by Monte Carlo computations.

The code is based on the GEANT-4 package; it models the shields, the cryostat, the detector structure and the detector array. It includes the propagation of photons, electrons, alpha particles and heavy ions (nuclear recoils from alpha emission) as well as neutrons and muons. For radioactive chains or radioactive isotopes alpha, beta and gamma and X-rays emissions are considered according to their branching ratios. The time structure of the decay chains is taken into account and the transport of nuclear recoils from alpha emissions is included.

The background sources considered are:

(1) bulk and surface contamination of the construction materials from the ^{238}U, ^{232}Th chains and ^{40}K and ^{210}Pb isotopes;
(2) bulk contamination of construction materials due to cosmogenic activation;
(3) neutron and muon flux in the Gran Sasso Laboratory;
(4) gamma ray flux from natural radioactivity in the Gran Sasso Laboratory, and
(5) background from the 2νββ decay.

The main contribution to background from bulk contaminants comes from the heavy structures near the detectors (the copper mounting structure of the array, the Roman lead box and the two lead disks on the top of the array) and from the TeO$_2$ crystals themselves. The radioactivity levels used in the computations for these materials are given in Table 1. The ^{232}Th, ^{238}U, ^{40}K and ^{210}Pb contamination levels of TeO$_2$, copper and lead, as well as the ^{60}Co cosmogenic contamination of copper, are deduced from the 90% CL upper limits obtained for the contaminations measured in MI-DBD experiment and with low-activity Ge spectrometry [45]. In both cases, no evidence of a bulk contamination was detected with the achievable sensitivity and only upper limits could be obtained. On the other hand, the ^{60}Co cosmogenic contamination of TeO$_2$ was evaluated according to the

Table 1
Bulk contamination levels in picograms per gram

Contaminant	^{232}Th	^{238}U	^{40}K	^{210}Pb	^{60}Co
TeO$_2$	0.5	0.1	1	10 µBq/kg	0.2 µBq/kg
Copper	4	2	1	0	10 µBq/kg
Roman lead	2	1	1	4 mBq/kg	0
16 Bq/kg lead	2	1	1	16 Bq/kg	0

Table 2
Computed background in the 0νββ decay and in the low-energy regions for bulk contaminations in the different elements

Simulated element	TeO$_2$ crystals	Cu structure	Pb shields	Total
0νββ decay region (counts/(keV kg year))	1.6×10^{-3}	1.5×10^{-3}	7.0×10^{-4}	3.8×10^{-3}
Dark matter region (counts/(keV kg day))	2.3×10^{-2}	9.6×10^{-4}	5.0×10^{-5}	2.4×10^{-2}

The Cu structure accounts for the detector mounting structure and the 50 mK shield.

time required to produce TeO$_2$ powder from the ore, grow the crystals and store them underground. The results of the Monte Carlo simulations using these contamination levels are given in Table 2 for the 0νββ decay and the low-energy (10–50 keV) regions. The threshold is assumed to be 10 keV and only values after reduction by anti-coincidence between detectors are indicated. These values have to be considered as upper limits on the possible contribution of bulk contaminations to the CUORE background; they prove that with the already available materials background lower than $\sim 4 \times 10^{-3}$ counts/(keV kg year) in the 0νββ decay region and $\sim 3 \times 10^{-2}$ counts/(keV kg day) in the low-energy (10–50 keV) region will be achieved.

Surface contaminations contribute to background only when they are localized on the crystals or on the copper mounting structure directly facing them. Background contributions in the two regions of interest are summarized in Table 3. There U and Th contaminations with an exponential density profile and a $\sim 1\,\mu m$ depth (in agreement with the contaminations observed in the MI-DBD experiment) are considered, while the contamination of this surface layer is assumed to be ~ 100 times smaller for the TeO$_2$ crystals and ~ 50 times smaller for copper than the corresponding contamination in MI-DBD experiment. As discussed in Section 4 the MI-DBD crystals were contaminated during the polishing procedure due to the use of highly contaminated powders. Polishing powders with a radioactive content 1000 times lower are, however, commercially available (Admatechs Co. Ltd., Japan) and have already been used for Cuoricino. An improvement of the surface contamination by a factor 100 is,

Table 3
Computed background in the 0νββ decay and in the low-energy regions for surface contaminations

Simulated element	TeO$_2$ crystal	Cu mounting structure	Total
0νββ decay region (counts/(keV kg year))	8.5×10^{-4}	2.0×10^{-3}	2.8×10^{-3}
Dark matter region (counts/(keV kg day))	6.8×10^{-4}	5.3×10^{-4}	1.2×10^{-3}

therefore, fully justified. A similar situation is that of copper; in the MI-DBD experiment, the copper surfaces were treated with an etching procedure [46] shown to reduce impurities on surfaces before the sputtering process. This procedure significantly improved the surface quality of copper; however, it is not optimized from the point of view of background. The use liquids with low levels of contamination (water and inorganic acids are available with U and Th contaminations lower than 0.1 pg/g) in a low background environment will allow an improvement of one to two orders of magnitude in the surface contamination of copper.

Other background sources, i.e. cosmogenic activation as well as muons, neutrons and gamma rays from the laboratory environment should produce minor contributions to the 0νββ background by virtue of the underground storage of construction materials and the optimization of the lead and neutron shields.

In particular, the only cosmogenically produced long-lived isotope contributing to 0νββ background is ^{60}Co whose presence has been already included as a bulk contamination of both TeO$_2$ and copper (see Tables 1 and 2). The situation is a little different in the low-energy region. A

preliminary evaluation of the non-intrinsic background rates near threshold results in a counting rate similar to that due to bulk contaminations. A complete and detailed study of the non-intrinsic background rates is underway.

Using the present upper limits for the ^{130}Te 2ν half-life, the unavoidable background produced by the 2νββ decay is lower than 10^{-4} counts/(keV kg day) in the low-energy region (using the predicted energy resolution).

In summary, in a very conservative approach where the CUORE-tower mechanical structure is assumed to be identical to that of CUORICINO, and with the presently achieved quality of low-contamination materials, and considering the worst possible condition for bulk contaminations (i.e. all the contamination equal to the present 90%, CL measured upper limits (Table 1), the CUORE background will be ~ 0.007 counts/(keV kg year) at the 0νββ transition and ~ 0.05 counts/(keV kg day) near threshold.

7.2. Background R&D for CUORE

The construction of CUORE will require about 5 years; during that period we plan to spend significant effort to further reduce the background. There are indeed several points on which it is possible to work. Concerning the crystals, their 1.8×10^{-3} counts/(keV kg year) contribution to the 0νββ region is dominated by the ^{60}Co cosmogenic contamination. This could be lowered by one order of magnitude by producing the crystals in a shallow depth laboratory. For U and Th impurities, we have only upper limits of the order 10^{-13} g/g. However, we know that before crystallization the TeO$_2$ powder is much more contaminated; therefore, the selection of a lower contamination powder together with the efficient reduction of impurities by multiple crystallization procedures should guarantee a contamination of 10^{-14} g/g. The situation for copper is different; not only it is possible to select low-contamination copper, but it is also possible to reduce the amount of copper used for the mounting structure of the detectors. This is particularly true in the case of the two copper frames (see Fig. 5) that hold the crystals in the four-detector module. In

CUORICINO (and also in our simulation), they are more massive than necessary from both the thermal and the mechanical points of view. A reduction of their mass and surface by at least a factor of two is possible with a consequent reduction of the bulk and surface contribution to background. The background coming from surface contaminations is dominated, in the 0νββ region, by the copper contribution and mainly by the four-crystal copper frames.

This contribution could be reduced not only by the reduction of the mass of the frame but also by covering the copper surfaces with cleaner materials. If successful this R&D would then result in a reduction of background to the level of 0.001 counts/(keV kg year) at the 0 νββ transition energy and to 0.01 count/(keV kg day) at threshold.

7.3. CUORE 0νββ sensitivity

The connection between the effective electron neutrino mass and the nuclear structure factor F_N is given in Eq. (4). The values of F_N calculated for ^{76}Ge and ^{130}Te are given in Table 4 for 11 different nuclear structure models.

It is evident from the values in Table 4 that for a given half-life sensitivity, a ^{130}Te detector can be between a factor of ~ 2 and ~ 4.6 as efficient in

Table 4
Computed values of $F_N \equiv G^{0\nu}|M_f^{0\nu} - (g_A/g_V)^2 M_{GT}^{0\nu}|^2$ for ^{76}Ge and ^{130}Te and the $\langle m_\nu \rangle$ ^{130}Te sensitivity for $\tau_{1/2} = 2 \times 10^{26}$ year

$F_N(^{76}\mathrm{Ge})$	$\dfrac{F_N(^{130}\mathrm{Te})}{F_N(^{76}\mathrm{Ge})}$	$F_N(^{130}\mathrm{Te})$	$\langle m_\nu \rangle$	Refs.
1.12×10^{-13}	4.76	5.33×10^{-13}	0.050	[47]
1.12×10^{-13}	4.32	4.84×10^{-13}	0.052	[48]
1.87×10^{-14}	21.20	3.96×10^{-13}	0.057	[49]
1.54×10^{-13}	10.58	1.63×10^{-12}	0.028	[50]
1.13×10^{-13}	9.74	1.1×10^{-12}	0.035	[51]
1.21×10^{-13}	4.13	5.0×10^{-13}	0.051	[52]
7.33×10^{-14}	4.09	3.0×10^{-13}	0.067	[53]
1.42×10^{-14}	8.73	1.24×10^{-13}	0.103	[53]
5.8×10^{-13}	5.48	3.18×10^{-12}	0.020	[54]
1.5×10^{-14}	—	—		[55]
9.5×10^{-14}	3.79	3.6×10^{-13}	0.060	[56]

probing the Majorana mass parameter, $\langle m_\nu \rangle$, as a ^{76}Ge detector. However, because of the ratio of the molecular weights and the ratio of the isotopic abundances in the detector materials, there are 5.41 times as many ^{76}Ge atoms in a kg of Ge metal isotopically enriched to 86% in ^{76}Ge, as there are ^{130}Te atoms in a kg of natural abundance TeO_2. If we drop the two highest and two lowest ratios in Table 4 and average the remaining ratios, we find $\langle F_N(^{130}\text{Te})/F_N(^{76}\text{Ge})\rangle \simeq 6.2$. Considering the uncertainty in this procedure, we estimate that a detector of TeO_2 of natural abundance is equivalent in decay rate to one of 86% ^{76}Ge of the same mass.

CUORE will have 206 kg of ^{130}Te which will contain 1.19×10^{27} atoms of ^{130}Te. If we assume, from our discussion of backgrounds, a counting rate of 0.01 counts/(keV kg year) and an energy resolution of ~ 5 keV, there will be less than 60 background counts/kg year to a 95% confidence level in the 5 keV window. The half-life sensitivity is given by

$$T_{1/2}^{0\nu}(^{130}\text{Te}) \geqslant (8.25 \times 10^{26})\left(\frac{t}{2\sqrt{BG}}\right) \text{ years.} \qquad (9)$$

The total number of background counts expected in the 5 keV window in 10 years is ~ 460. The 1σ statistical fluctuation, $\sigma = \sqrt{n}$, is ~ 21 and the 2σ CL is 42. The half-life sensitivity is then $\sim 2 \times$

10^{26} years. Using Eq. (4), we quote the sensitivities of the Majorana mass parameter in the last column of Table 4.

Assuming that a background of 0.001 counts/(keV kg year) would be reached, the 10-year sensitivity would be $\sim 3.5 \times 10^{26}$ years (at 95% CL) and the corresponding sensitivities of the Majorana mass parameter will be ~ 1.8 times higher than those quoted in Table 4 (i.e. in the range 11–56 meV). This is in the region of neutrino mass where oscillation experiments imply then could well be an observation.

7.4. CUORE dark matter and axion sensitivity

The sensitivity of CUORE in WIMP detection is shown in Fig. 12 where the 1-year projected exclusion plots for background counting rates of 0.05 and 0.01 counts/(keV kg day) and a threshold of 10 keV are shown. Thanks to the large mass of the detector, CUORE will be also be able to give results on the dark matter modulation signal as discussed in Ref. [57]. Concerning solar axion detection the sensitivity of CUORE will depend strongly on the threshold reached. In the case of a 5 keV threshold and a 2 keV FWHM low-energy resolution, the $g_{\gamma\gamma}^{\lim}$ sensitivity is about 7×10^{-10} GeV^{-1} [26]. A lower threshold would be highly desirable for this application.
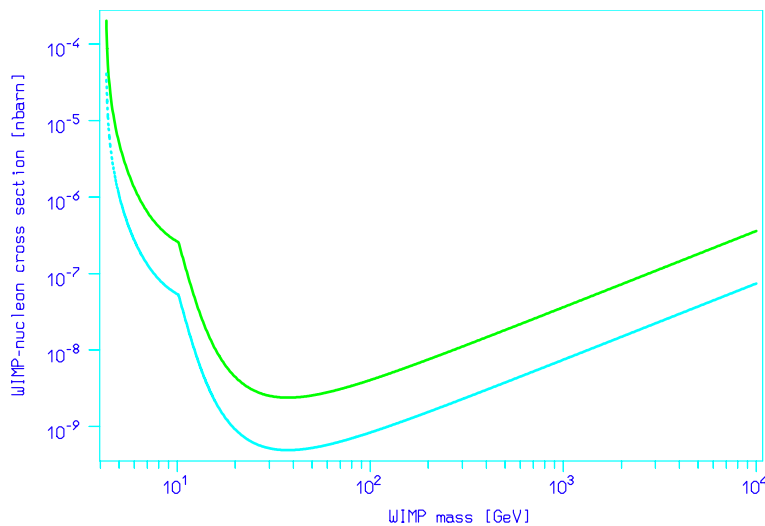

Fig. 12. Exclusion plots for a background of 0.05 and 0.01 counts/(keV kg day).

8. The enrichment option

CUORE is the only proposed next generation a $0\nu\beta\beta$ decay experiment that plans the use of non-enriched material. Indeed, the high isotopic abundance of ^{130}Te allows very high sensitivities even using the much cheaper natural abundant material. This obviously implies that the construction of a larger array would not only be technically possible but also fiscally acceptable. On the other hand, the high natural abundance of ^{130}Te allows a much simpler and less expensive enrichment procedure than that for other double-beta decay candidates. Moreover, TeO$_2$ crystals made with ^{130}Te isotopically enriched material have been already tested during the MI-DBD experiment with results consistent with those obtained for natural crystals, both from the point of view of detector performance and detector background. An enriched CUORE with a background of 0.001 counts/(keV kg year) would have a 10-year half-life sensitivity of $\sim 10^{27}$ years (at 95% CL) implying a sensitivity on the Majorana mass parameter in the range 9–46 meV.

9. Conclusions

It is quite straightforward to demonstrate how the determination of the effective Majorana mass of the electron neutrino constrains the lightest neutrino mass eigenvalue. This was done recently by Barger et al. [58]. However, it is very convenient to use the approximation that $\sin\theta_2 \simeq 0 \equiv s_2$ and $\cos\theta_2 \simeq 1$. With the further observation that $\delta m_\odot^2 \ll \delta m_{AT}^2$ in the normal hierarchy case we obtain

$$|\langle m_v \rangle| \leqslant m_1 \leqslant \frac{|\langle m_v \rangle|}{\cos(2\theta_3)} \tag{10}$$

where $\cos(2\theta_3) \simeq 0.5$. Similarly, in the case of inverted hierarchy

$$\sqrt{|\langle m_v \rangle|^2 - \delta m_{AT}^2}$$
$$\leqslant m_1 \leqslant \sqrt{\frac{|\langle m_v \rangle|^2 - \delta m_{AT}^2 \cos(2\theta_3)}{\cos(2\theta_3)}}. \tag{11}$$

A related quantity, $\Sigma \equiv m_1 + m_2 + m_3$ has great importance in cosmology. It is related to the quantity Ω_v, the fraction of the critical density, ρ_0 (that would close the universe) that is in the form of neutrinos, where

$$\Sigma = (93.8 \text{ eV}) \ \Omega_v h^2 \tag{12}$$

and h is the dimensionless Hubble constant. It was shown in Ref. [58] that Σ obeys the following inequality with respect to $|\langle m_v \rangle|$:

$$2|\langle m_v \rangle| + \sqrt{|\langle m_v \rangle|^2 \pm \delta m_{AT}^2}$$
$$\leqslant \Sigma \leqslant \frac{2|\langle m_v \rangle| + \sqrt{|\langle m_v \rangle|^2 \pm \delta m_{AT}^2 \cos(2\theta_3)}}{\cos(2\theta_3)} \tag{13}$$

where the $+$ and $-$ signs refer to normal and inverted hierarchy, respectively, and $\cos(2\theta_3) \equiv$ 0.5. If this relation is written as two equalities, and each side is solved for $|\langle m_v \rangle|$ in terms of Σ, quadratic equations result with constant terms ($\Sigma^2 \mp \delta m_{AT}^2$). Values of Σ of cosmological interest are much larger than $\delta m_{AT}^2 \leqslant 0.005$ eV (99.73% CL). Accordingly, the above inequality reduces to the trivial form

$$|\langle m_v \rangle| \leqslant \Sigma/3 \leqslant 2|\langle m_v \rangle|. \tag{14}$$

This clearly demonstrates the direct connection between neutrinoless double-beta decay and neutrino dark matter. Cosmic microwave background and galaxy cluster surveys have set the bound $\Sigma \leqslant 1.8$ eV [59]. It is expected that the MAP satellite will produce data that will result in a sensitivity $\Sigma \simeq 0.5$ eV. In the case of Majorana neutrinos, the CUORE experiment is projected to have a sensitivity of $\Sigma \simeq (0.035–0.103)$ eV depending on the nuclear matrix element used to analyze the data.

One interesting scenario results if the MAP or a future satellite, for example, observes a clear signal well above their limiting sensitivity, and CUORE (as well as other next generation experiments) has a negative result at sensitivities of Σ far below that of the satellite data. This would be a clear indication that the phenomenon causing the density fluctuations implied by the CMB data was not caused by Majorana neutrino dark matter. In addition, a positive measurement of the mass

m_{ν_e} by KATRIN ^{3}He beta end-point spectrum measurement would have to yield $m_{\nu_e} \leqslant 0.35$ eV. The CUORE experiment will have a far greater sensitivity, and if it finds a negative result, the mystery of the Dirac or Majorana character of neutrinos will be solved.

It should be abundantly clear from the forgoing discussion that the most important remaining issue in neutrino physics is the determination of the neutrino mass scale. Neutrino oscillation experiments have clearly demonstrated that

(1) neutrinos have mass and that their mass eigenstates mix,
(2) the mixing matrix elements have values that imply that next generation $0\nu\beta\beta$ decay experiments should be able to determine the scale of neutrino mass in the case of Majorana neutrinos.

The main advantage of CUORE is that it will utilize TeO$_2$ crystals of natural isotopic abundance Te, while also this technology has yielded energy resolutions approaching those of intrinsic Ge detectors. Energy resolution is crucially important for an actual observation of $0\nu\beta\beta$ and a measurement of $|\langle m_\nu \rangle|$.

Note added in proof

Since the submission of this paper, the CUOR-ICINO detector has operated, and has thus far yielded the following bounds: $T_{1/2}^{0\nu}(^{130}\text{Te}) \geqslant 5.5 \times 10^{23} y$, corresponding to $\langle m_\nu \rangle \leqslant (0.37-1.9)$ eV, depending on the nuclear model used to extract the effective Majorana mass.

References

[1] W.H. Furry, Phys. Rev. 56 (1939) 1184.
[2] H. Primakoff, S.P. Rosen, Rep. Prog. Phys. 22 (1959) 121;
H. Primakoff, S.P. Rosen, Phys. Rev. 184 (1969) 1925;
G.F. Dell'Antonio, E. Fiorini, Suppl. Nuovo Cimento 17 (1960) 132.
[3] W.C. Haxton, G.J. Stevenson Jr., Prog. Part. Nucl. Phys. 12 (1984) 409;
F.T. Avignone III, R.L. Brodzinski, Prog. Part. Nucl. Phys. 21 (1988) 99;
M. Moe, P. Vogel, Ann. Rev. Nucl. Part. Sci. 44 (1994) 247.
[4] A. Morales, Nucl. Phys. B 77 (Proc. Suppl.) (1999) 335;
H. Ejiri, Phys. Rep. C 338 (2000) 265;
H. Ejiri, Int. J. Mod. Phys. E 6 (1997) 1;
V. Tretyak, Y. Zdesenko, At. Data, Nucl. Data Tables 80 (2002) 93.
[5] S. Elliott, P. Vogel, Ann. Rev. Nucl. Part. Sci. 52 (2002) 115.
[6] E. Fiorini, et al., Phys. Lett. B 25 (1967) 602;
E. Fiorini, et al., Lett. Nuovo Cimento 3 (1970) 149.
[7] A.A. Vasenko, et al., Mod. Phys. Lett. A 5 (1990) 1299;
F.T. Avignone, et al., Phys. Lett. B 256 (1991) 559.
[8] L. Baudis, et al., Phys. Rev. Lett. 83 (1999) 41.
[9] C.E. Aalseth, et al., Phys. Rev. C 59 (1999) 2108;
C.E. Aalseth, et al., Yad. Fiz. 63 1299 (2000) 1341;
C.E. Aalseth, et al., Phys. At. Nucl. 63 (2000) 1225,1268;
D. Gonzales, et al., Nucl. Phys. B 87 (Proc. Suppl.) (2000) 278.
[10] C.E. Aalseth, et al., Phys. Rev. D 65 (2002) 092007.
[11] Y. Fukuda, et al., Phys. Rev. Lett. 82 (1999) 1810;
Y. Fukuda, et al., Phys. Rev. Lett. 82 (1999) 2430;
Y. Fukuda, et al., Phys. Rev. Lett. 82 (1999) 2644.
[12] W. Hampel, et al., The GALLEX Collaboration, Phys. Lett. B 388 (1996) 384;
G.N. Abdurashitov, et al., The SAGE Collaboration, Phys. Rev. Lett. 77 (1996) 4708;
B.T. Cleveland, et al., Astrophys. J. 496 (1998) 505;
R. Davis, Prog. Part. Nucl. Phys. 32 (1994) 13;
Y. Fukuda, et al., Phys. Rev. Lett. 86 (2001) 5651;
Y. Fukuda, et al., Phys. Rev. Lett. 86 (2001) 5656.
[13] Q.R. Ahmad, et al., Phys. Rev. Lett. 87 (2001) 071301;
S. Fakuda, et al., Phys. Lett. B 539 (2002) 179, arXiv:hep-ex/0205075.
[14] S. Pascoli, S.T. Petcov, L. Wolfenstein, Phys. Lett. B 524 (2002) 319–331.
[15] F. Feruglio, A. Strumia, F. Vissani, hep-ph/0201291;
F. Feruglio, A. Strumia, F. Vissani, Nucl. Phys. B 637 (2002) 345.
[16] S.M. Bilenky, S. Pascoli, S.T. Petcov, arXiv: hep-ph/0105144 v1 15 May 2001;
S.M. Bilenky, S. Pascoli, S.T. Petcov, Phys. Rev. D 64 (2001) 053010.
[17] S. Pascoli, S.T. Petcov, arXiv: hep-ph/0205022.
[18] H.V. Klapdor-Kleingrothaus, H. Ps, A.Yu. Smirnov, Phys. Rev. D 63 (2001) 073005.
[19] S.M. Bilenky, C. Guinti, W. Grimus, B. Kayser, S.T. Petcov, Phys. Lett. B 465 (1999) 193;
Y. Farzan, O.L.G. Peres, Y. Smirnov, Nucl. Phys. B 612 (2001) 59.
[20] A. Alessandrello, et al., Phys. Lett. B 486 (2000) 13;
C. Arnaboldi, et al., A calorimetric search on double beta decay of ^{130}Te, Phys. Lett. B 557 (2003) 167.
[21] D. Twerenbold, Rep. Prog. Phys. 59 (1996) 349;
N. Booth, B. Cabrera, E. Fiorini, Ann. Rev. Nucl. Sci. 46 (1996) 471.
[22] E.E. Haller, et al., in: R.D. Larrabee (Ed.), Proceedings of the Fourth International Conference on Neutron Trans-mutation Doping of Semiconductor Materials, National

Bureau of Standards, June 1,2, 1982, Gaithersburg, MD, Plenum Press, New York, 1984, p. 21.

[23] E. Norman, R.J. McDonald, Presentation made to the CUORE collaboration, Milan, Italy, 11 December 2000, private communication.

[24] A. Alessandrello, et al., Nucl. Phys: Russ. Acad. Sci., in press, arXiv: hep-ex/0201038.

[25] A. Alessandrello, et al., Nucl. Phys. B 87 (Proc. Suppl.) (2000) 78.

[26] R.J. Creswick, et al., Phys. Lett. B 427 (1998) 235;
F.T. Avignone III, et al., Phys. Rev. Lett. (1998) 5068;
S. Cebrian, et al., Astropart. Phys. 10 (1999) 397.

[27] M. Barucci, et al., J. Low Temp. Phys. 123 (2001) 303.

[28] G.K. White, S.J. Collocott, J.G. Collins, J. Phys.: Condens. Matter 2 (1990) 7715.

[29] A. Giuliani, S. Sanguinetti, Mater. Sci. Eng. R 11 (1993) 52.

[30] N.F. Mott, Philos. Mag. 19 (1969) 835.

[31] B.I. Shklovskii, A.L. Efros, Sov. Phys. JETP 33 (1971) 468.

[32] A. Alessandrello, et al., J. Phys. D 32 (1999) 3099.

[33] F. Pobell, Matter and Methods at Low Temperatures, Springer, Berlin, 1992.

[34] A. Alessandrello, et al., in: S. Cooper (Ed.), Proceedings of the Seventh International Workshop on Low Temperature Detectors (LTD7), Munich, Germany, Springer, Berlin, 27 July–2 August 1997, p. 249.

[35] A. Alessandrello, et al., Nucl. Instr. and Meth. B 142 (1998) 163.

[36] C. Arnaboldi, et al., The programmable front-end system for cuoricino, an array of large-mass bolometers, IEEE Trans. Nucl. Sci. 49 (2002) 2440.

[37] C. Arnaboldi, et al., Low frequency noise characterization of very large value resistors, IEEE Trans. Nucl. Sci. 49 (2002) 1808.

[38] J.C. Mather, Appl. Opt. 21 (1982) 1125;
R.C. Jones, J. Opt. Soc. Am. 43 (1953) 1.

[39] A. Fascilla, G. Pessina, Nucl. Instr. and Meth. A 469 (2001) 116.

[40] G. Pessina, Rev. Sci. Instrum. 70 (1999) 3473.

[41] C. Liguori, G. Pessina, Nucl. Instr. and Meth. A 437 (1999) 557.

[42] C. Arnaboldi, G. Pessina, A very simple baseline restorer for nuclear applications, Nucl. Instr. and Meth. A 512 (2003) 129.

[43] E. Gatti, P.F. Manfredi, Rivista Nuovo Cimento 9 (1) (1986) 1.

[44] A. Alessandrello, et al., Nucl. Instr. and Meth. A 412 (1998) 454.

[45] G. Heusser, private communication.

[46] V. Palmieri, et al., Electropolishing of seamless 1.5 GHz OFHC copper cavities, in: B. Bonin (Ed.), Proceedings of the Seventh Workshop on RF Superconductivity, Gif Sur Yvette, France 1995, DIST CEA/SACLAY 96 080/1,2, 605;
V. Palmieri, et al., Besides the standard Niobium bath chemical polishing, Proceedings of the 10th Workshop on RF Superconductivity, September 6–11 2001, Tsukuba, Japan, 2002, in press.

[47] A. Staudt, et al., Europhys. Lett. 13 (1990) 31.

[48] T. Tomoda, Rep. Prog. Phys. 54 (1991) 53.

[49] P. Vogel, et al., Phys. Rev. Lett. 57 (1986) 3148;
P. Vogel, et al., Phys. Rev. C 37 (1988) 73.

[50] S.M. W.C. Haxton, et al., Prog. Part. Nucl. Phys. 12 (1984) 409;
W.C. Haxton, et al., Nucl. Phys. B 31 (Proc. Suppl.) (1993) 82;
W.C. Haxton, et al., Phys. Rev. D 26 (1982) 1085.

[51] J. Engel, P. Vogel, Phys. Rev. Lett. B 225 (1989) 5.

[52] O. Civitaresa, A. Faessler, T. Tomoda, Phys. Lett. B 194 (1987) 11;
T. Tomoda, A. Faessler, Phys. Lett. B 199 (1987) 473;
J. Suhonen, O. Civitarese, Phys. Rev. C 49 (1994) 3055.

[53] A. Pantis, et al., Phys. Rev. C 53 (1996) 695.

[54] A. Staudt, Kuo, H. Klapdor, Phys. Rev. C 46 (1992) 871.

[55] E. Caurier, et al., Phys. Rev. Lett. 77 (1996) 54;
Retamosa, et al., Phys. Rev. C 51 (1995) 371;
A. Poves, et al., Phys. Lett. B 361 (1995) 1.

[56] J.G. Hirsch, et al., Nucl. Phys. A 589 (1995) 445;
C.R. Ching, et al., Phys. Lett. B 272 (1991) 169;
C.R. Ching, et al., Phys. Lett. B 276 (1992) 274.

[57] S. Cebrian, et al., arXiv: hep-ph/9912394, Astropart. Phys. 9 (2001) 339.

[58] V. Barger, S.L. Glashow, D. Marfatia, K. Whisnant, Phys. Lett. B 532 (2002) 15.

[59] O. Ergaroy, et al., Phys. Rev. Lett. 89 (2002) 061301, arXiv: astro-ph/0204152.